16

Broadband anti-reflective composite coating: effect of pulsed laser treatment on optical properties

© F.F. Komarov[1], M.N. Zhukava[1,*], O.V. Milchanin[1], O.R. Lyudchik[2]

[1] A.N. Sevchenko Institute of Applied Physics Problems,
Minsk, Belarus
[2] Belarusian State University,
Minsk, Belarus

e-mail: maryliss.lab@gmail.com

Received March 12, 2024
Revised April 25, 2024
Accepted May 20, 2024

The developed method of laser treatment for the formation of antireflective coatings on the basis of composite materials created by filling epoxy polymer with multi-walled carbon nanotubes has been demonstrated. The influence of surface structuring of composite materials by pulsed laser treatment on reflectivity in UV-, visible- and IR wavelength ranges ($0.2-25\,\mu$m) has been investigated. A composite material was created and structures with low reflectance in the specified wavelength range were formed on it. Optical characteristics of such structures meet the standard requirements for anti-reflection coatings of optoelectronic and optical systems of aerospace vehicles.

Keywords: multi-walled carbon nanotubes, epoxy polymer, composite material, pulsed laser treatment, structuring, broadband antireflective coatings.

DOI: 10.61011/EOS.2024.06.59536.6139-24

Introduction

Materials weakly reflecting in a wide spectral range of electromagnetic radiation (EMR) are of great interest. They are used as coatings in aerospace optical and optoelectronic systems, photovoltaic cells, thermo/photodetector systems, for military stealth solutions, in particular, in UAV. The existing literature describes many material reflectivity reduction options [1–6], for example, by adding absorbing agents such as dyes, carbon particles, gold and platinum black particles to the structure of materials [1,7–10]. It should be noted that the air/surface interface imposes strong restrictions on the incident radiation portion that may be absorbed. To solve this problem and minimize the reflection of incident radiation on the composite material surface, an antireflective layer is created through formation of subwavelength discontinuities [11–15]. In this case, the EMR refraction index in the near-surface region of the layer and in the interfacing air (vacuum) region are of similar values ($\sim 1.0-1.1$).

Nowadays, a wide range of physical and chemical processes for fabrication of weakly reflecting coatings is used, including a number of methods for deposition and growing of carbon nanotube (CNT) arrays [10], ion-plasma etching [3–5,12,14,15], lithographic methods [13], deposition of low-density aerogel coatings and other porous coatings [1,16] and growing of vertically-aligned carbon nanotubes [6,10,17–19].

It should be noted that the emulation of natural functions of extreme black and antireflective systems in living organisms formed during evolution over many millions of years provided several effective antireflective coatings [19–23]. This is particularly true for structured coatings implemented using „moth eye“ [19,22,23] or „butterfly wing“ patterns [21]. In terms of optical characteristics, coatings based on vertically-aligned CNT arrays (VANTA) are currently the most effective anti-reflective systems in a wide spectral range from the visible to far IR range [10,17,24]. The refraction index of the VANTA material in air is close to 1 and its imaginary part is much lower than 1 [10]. Such material may be treated as a composite material consisting of a weakly reflective material and air.

However, these methods are not commercially applicable due to some disadvantages of each of them. Materials formed by ion and plasma etching cannot achieve the adequate control level for uniform large-scale replication of the structure. Aerogels have low mechanical resistance and the issue of toxic effect of products used in their production is critical. For single-walled carbon nanotube (SWCNT) arrays grown vertically by the CVD method on substrates with catalyst metal and having high anti-reflective properties in a wide spectral range [6,17,19], the main shortcoming is the complexity of growing process and low mechanical strength of systems to be grown. The lithographic printing method that uses special master molds is a well proven and quite simple method that does not require any expensive process equipment. However, fabrication of master molds that ensure a material surface topology change takes a long time and, therefore, constitutes a disadvantage because it is impossible to define simultaneously the required parameters for coating surfaces.

This study focuses on the surface structuring method for fabrication of anti-reflective coatings using pulsed laser radiation. The idea is in formation of a periodic structure

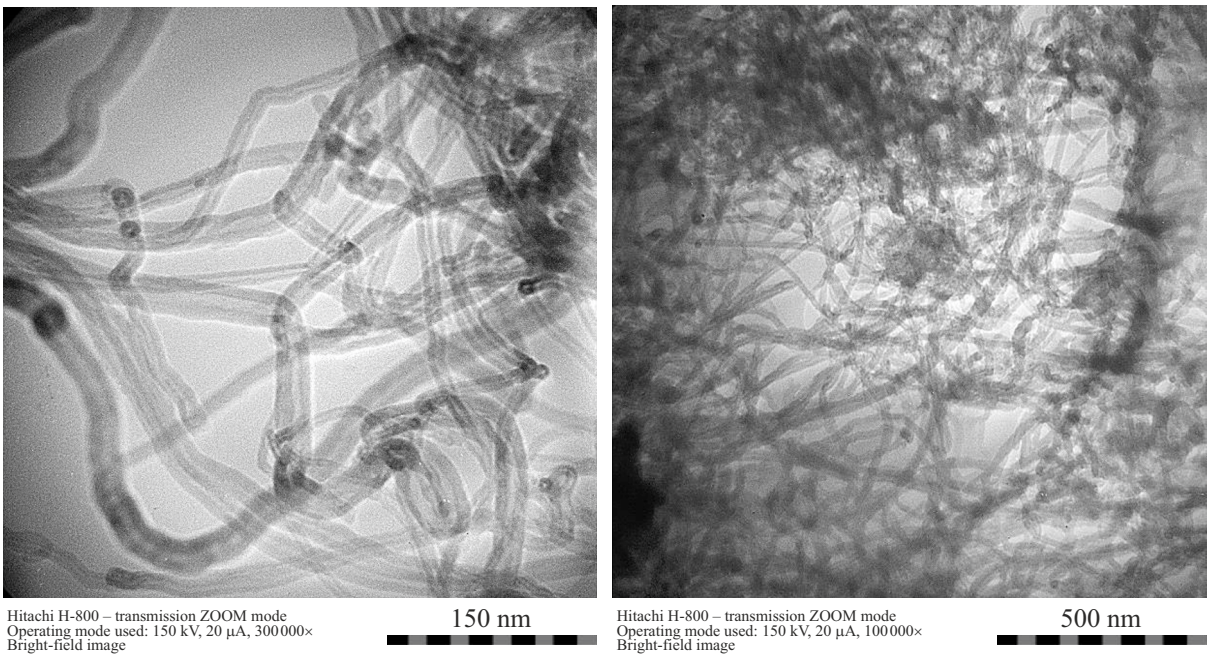

Figure 1. TEM microphotograph of the Taunite-M MWCNT structure (left) and formed composite material (right).

on the feedstock surface by laser beam scanning according a pre-set sequence with partial removal of material. Such approach provides control of dimensions (width, depth, degree of wall roughness) and spacing of the grooves to be formed. The composite was fabricated from an epoxy polymer filled with a pre-defined concentration of multi-walled carbon nanotubes (MWCNT). Graphene-like MWCNT structures ensure high EMR absorption efficiency and allow volume absorbing meshes to be formed in the used polymer [15]. Low cost of MWCNT compared with single-walled CNT shall be also emphasized.

Experiment procedure

Fabrication of a structured coating featuring low absorption coefficient included two main procedures: fabrication o a composite specimen from polymer with MWCNT addition and then laser surface treatment of the composite specimen. Six types of specimens were prepared. ED-20 epoxy resin was used as the polymer base. Taunite-M carbon nanotubes made by „NanoTechCenter“ (Tambov, Russia) were used as an additive. These multi-walled carbon nanotubes have the inside diameter of 5−10 nm, outside diameter of 10−30 nm and a length from 1 to 10 μm (Figure 1), geometrical surface is $> 160\,m^2/g$, thermal stability is up to 600°C [25].

Preparation of the composite material itself may be divided into 3 main stages.

1) Preliminary ultrasonic dispersion of multi-walled carbon nanotubes with 4 wt.% concentration in SAA alcohol solution (100 mM) to „disentangle“ the CNT coils and prevent clustering as well as to ensure uniform nanotube distribution throughout the composite material. The UP-400St ultrasonic homogenizer was used for solution dispersion. The process was performed at 24 kHz with an output power from 40 W to 80 W, with gradual increase in power from the minimum to maximum level to minimize defect formation in CNT and fragmentation.

2) Then the prepared solution was mixed with the epoxy polymer and again subjected to ultrasonic treatment.

3) At the final stage, after long-term dispersion (15−30 min), a curing agent was added to the solution and the finished specimen was polymerized in a drying cabinet at 65−70°C.

Surface profiling was performed by the 50 Hz 1064 nm pulsed Nd:YAG laser. Due to insufficient laser power (up to 100 mW) for burning a groove with the required depth in one pass on the surface, multiple passes were made in the same area to achieve the desired groove dimensions. The factors behind the anti-reflective surface properties of the composite material included: the pumping energy E_p, pulse frequency f, groove spacing h and laser beam focusing (on the surface or in depth). These factors ensure control of groove dimensions and shape as well as of groove wall topology. To form the periodic structure, parameters that provide the maximum depth, most uniform composite-air interface and lowest cavity bottom width were chosen — $E_p = 12.5$ and 13 J, beam focusing in depth and on the surface of the specimen, groove spacing $h = 100$ and 400 μm. After burning all tracks on the specimen, dust and composite spray particles that has accumulated during profiling shall be removed from the grooves. As long as the grooves are placed very close to each other and have small

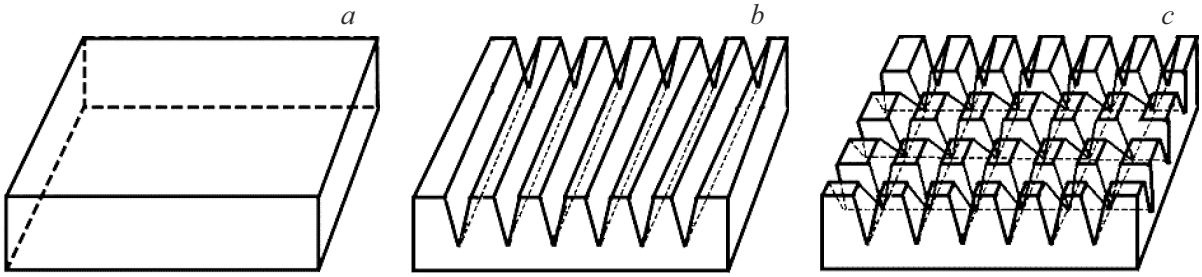

Figure 2. Schematic drawing of the specimen surface topologies: (a) topology of initial specimens, (b) topology of longitudinally profiled specimens, (c) topology of mesh-profiled specimens.

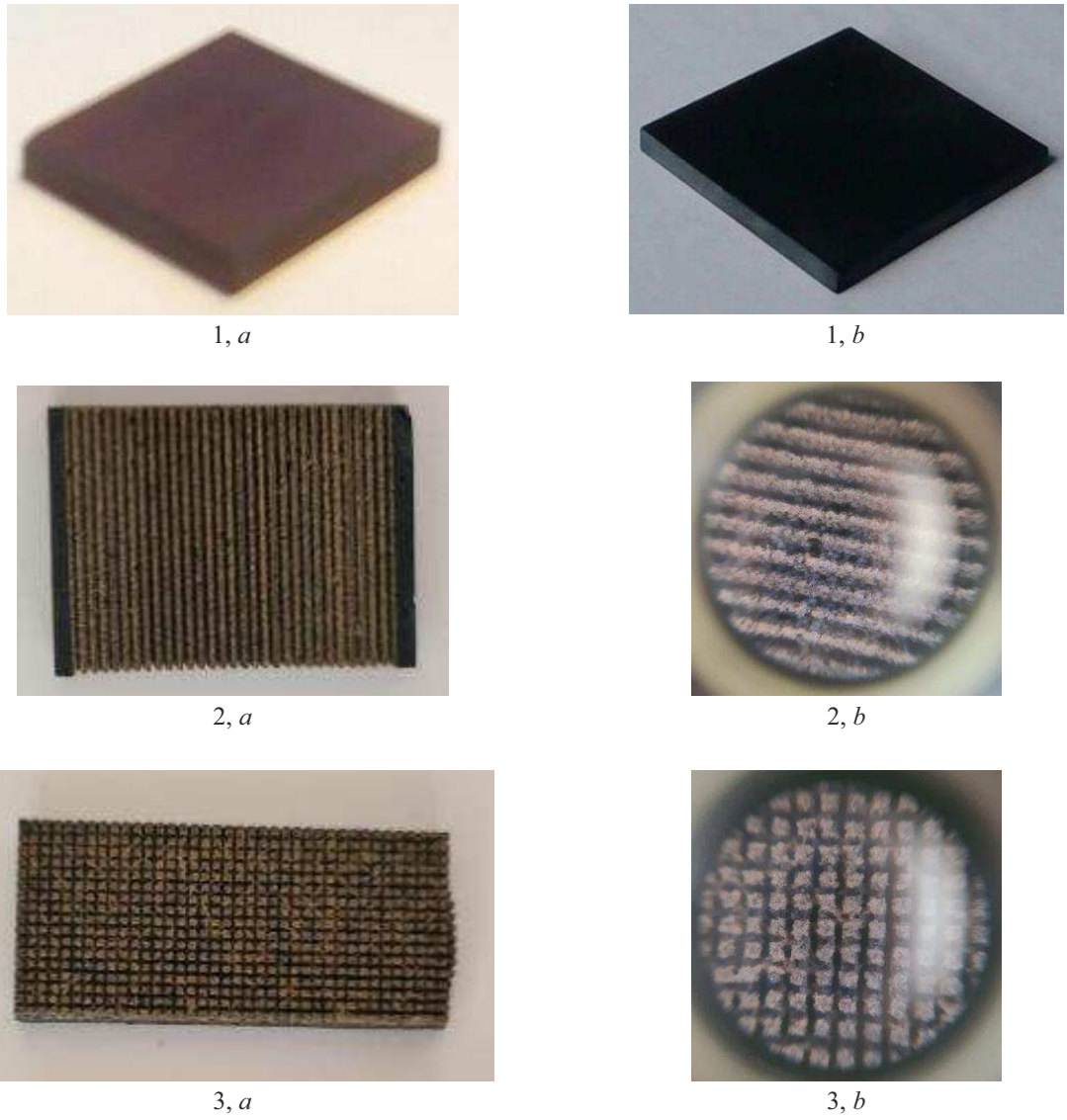

Figure 3. Photographs of the prepared polymer specimens: $1, a$ — initial polymer, $1, b$ — polymer filled with 4 wt.% Taunite-M CNT, $2, a, b$ — composite with groove-structured surface, $E_p = 12.5$ J, $3, a, b$ — composite with pyramid-structured surface, $E_p = 12.5$ J.

sizes, erosion products were removed from the near-surface area by pressure air blowing method.

Structural characteristics of the initial MWCNTs, carbon nanotube array distribution in the polymer matrix and surface morphology of the initial and laser treated composite were determined by the transmission and scanning electron microscopy using the Hitachi H-800 electron microscope and Hitachi H-8010 microscope, respectively. Reflectance

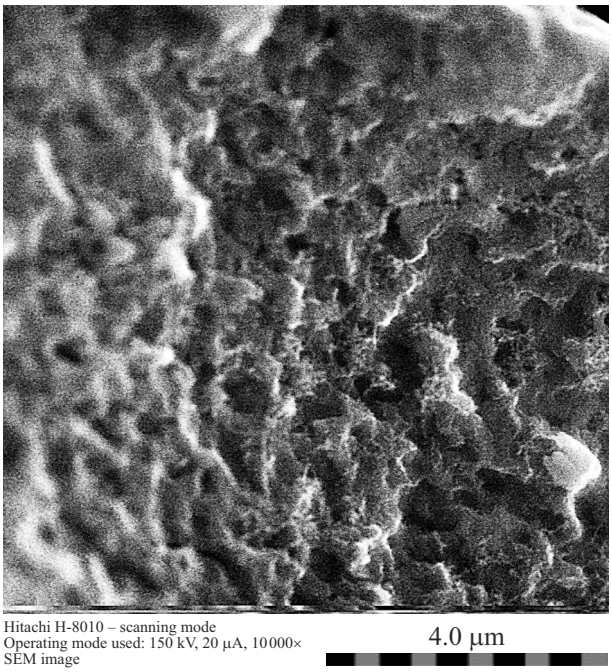

Figure 4. SEM image of the groove side wall in the composite material after laser treatment.

of the modified composite in the spectral range from 0.2 to $2.5\,\mu$m was recorded on the Lambda1050 spectrophotometer with a mirroring module and in the range of $2.5-25\,\mu$m on the Spectrum 3 Optica Fourier spectrophotometer.

Results and discussions

Figure 1 shows the TEM images of the initial Taunite-M CNT array and of the composite specimen filled with 4 wt.% Taunite-M nanotubes. The TEM microimage of the composite material shows a three-dimensional mesh of interlaced CNTs formed during fabrication and a polymer mesh structure with a mesh size$\sim$ 10 nm. Formation of a three-dimensional mesh within the polymer corresponds to the appearance of local regions that differ very much in electric conductivity, which may induce multiple EMR rereflection and refraction. Therefore, the fabricated composite will have high incident radiation absorption efficiency. Such features of EMR interaction with the composite materials have been already observed in the literature [1,7,10,15].

As mentioned above, the anti-reflective layer on the composite surface was formed by laser treatment with software-controlled multiple laser beam passes on the surface with the pre-defined groove spacing. The surface treatment process was followed by creation of a system of parallel grooves and further perpendicular treatment produced pyramidal structures (Figures 2 and 3).

As mentioned above the geometrical parameters of the grooves were controlled by the laser pumping energy, focal distance and number of passes per groove. As a result, a set of specimens with different topological parameters

Thickness of formed specimens

Specimens	Specimen thickness , mm
Epoxy polymer without MWCNT	2.5
Polymer with nanotube additives	3.2
Profiling conditions	
Lines 1 ($E_p = 12.5$ J)	2.95
Lines 2 ($E_p = 13.0$ J)	2.4
Mesh 1 ($E_p = 12.5$ J)	2.3
Mesh 2 ($E_p = 13.0$ J)	2.4

was made in accordance with the laser exposure conditions (Figure 3).

Laser treatment of the composite material provides formation of cells with nonuniform shapes on the groove and pyramid side walls with sizes from 100 nm to 500 nm. Cells are air cavities surrounded by melted material areas (Figure 4).

Such feature of the three-dimensional groove or pyramid structure provides agreement of the EMR refraction indices of the laser-treated composite and air, and increase in the absorption efficiency due to multiple EMR rereflection on the walls of the formed structures.

The table shows one of the geometrical parameters of the specimens — specimen thickness. Thickness shall be measured to determine the efficiency of EMR absorption by the formed layers.

Note that laser treatment in the chosen conditions of the initial polymer, i.e. without adding carbon nanotubes, does not lead to formation of grooves on the specimen surface. Therefore the influence on reflectivity was not replaced during profiling of the specimen surface without adding carbon nanotubes.

Transmission spectra measurements in the epoxy polymer without MWCNT (Figure 5, *a*) indicate low absorbance in the spectral range of $0.5-2.2\,\mu$m (transmits up to 50% of radiation). At the same time, the transmission coefficient for the specimens with CNT without laser surface structuring does not exceed 0.04% (Figure 5, *b*) and are not higher than 0.01% for the samples with profiled surface. This quantity is the spectrometer detection limit, therefore the actual values may be even lower. This indicates the role of CNT in the EMR absorption processes in the spectral range of $0.2-2.5\,\mu$m.

Figure 6, *a* shows the measured specular reflectances in the spectral range of $0.2-25\,\mu$m for composite specimens with addition of 4 wt.% carbon nanotubes with structured surface by the pulsed laser irradiation method with a structuring interval of $h = 400\,\mu$m. In a more expanded scale in Figure 6, *b* and 6, *c* shows the measured reflectances in the range of $0.2-2.5\,\mu$m in two laser pumping energy conditions (12.5 J and 13 J) and two groove spacings (400 and $100\,\mu$m, respectively). Reflection spectra of the initial polymer (specimen N1) and composite material filled with MWCNT (specimen N2)

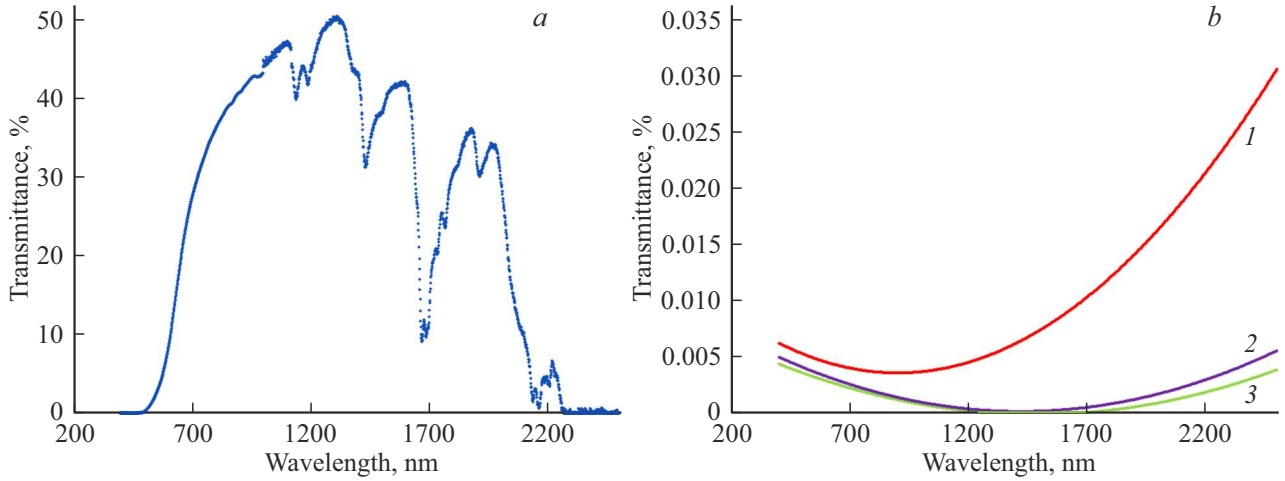

Figure 5. Transmission spectra of the initial polymer (a) and MWCNT-containing specimens (b): *1* — without laser treatment, *2* — with surface treatment for the parallel groove topology, *3* — with treatment for pyramid formation.

without surface structuring are also shown for comparison.

MWCNT addition to the polymer provides significant reduction of the reflectances throughout the examined spectral ranges (Figure 6, a) and is particularly pronounced for $0.2-2.5\,\mu$m (Figure 6, b, c). At $10\,\mu$m, this decrease achieves ~ 4 (Figure 6, a). In the spectral range of $0.2-2.5\,\mu$m, CNT addition to the polymer causes the reflectance decrease by a factor from ~ 2 to ~ 3 (Figure 6, b). Composite surface structuring additionally reduces the radiation reflectance (by a factor of ~ 3) to tenths of percent depending on the laser irradiation parameters compared with the composite without surface profiling in the spectral range of $0.2-3\,\mu$m (Figure 6, a). Minimum EMR reflection throughout the range of $0.2-2.5\,\mu$m is observed on specimen № 4 with pyramid-like profiling at $E_p = 12$ J. In the middle IR range ($3-25\,\mu$m), a considerable effect of near-surface structuring is also observed (Figure 6, a). Here, reflectance reduction is equal to $1-2$ orders of magnitude. Whilst, reflection in the spectral range of $0.2-2.5\,\mu$m for the specimens with structured surface does not exceed 0.5%, and only for specimen N3, the reflectance in the range of $15-25\,\mu$m is at 1%.

In terms of reflectance reduction, pyramid-like laser structuring of the composite surface has particular advantages (Figure 6, c). Such influence of the type of structural elements has been also found for specimens N5 and N6, for which the reflected signal (0.03%) in the visible range for the pyramidal mesh is 0.04% as weak as for the grooved structures.

An important role of the groove spacing shall be also emphasized. Reduction of the structuring spacing from 400 to $100\,\mu$m (Figure 6, c) leads to significant decrease in the reflected signal intensity and at the same time reflectance equivalencies vary for various laser treatment conditions.

Formation of the special surface topology makes it possible to reduce reflection by $1-2$ order of magnitude depending on the laser treatment conditions (Figure 6, c). Thus, for specimen 3, the reflectance is not higher than 0.1% in the visible ($0.4-0.8\,\mu$m) range and varies from 0.04% to 0.07% in the near IR ($1-2.5\,\mu$m) range (Figure 6, c). For specimen 5, the visible range reflectance does not exceed 0.07%, and in the IR range the reflected signal is not recorded correctly at all due to inadequate spectrometer sensitivity.

In terms of fundamental optics, „vacuum“ in the near-surface area of a solid body provides EMR reflection suppression. According to the Fresnel law, light falling from air (refraction index $n_o = 1.0003$) normal to a solid body surface with the refraction index n is reflected from the surface with the reflectance R:

$$R = (n - n_o)^2/(n + n_o)^2. \qquad (1)$$

Therefore, reflection is significantly reduced when the refraction index of the body is close to that of air. However, for most solid bodies, $n > 1.4$ (as an example, or materials with low refractive index, in particular for MgF_2 1.38, for fluorine-containing polymers 1.3–1.4 [14]). Therefore, the reflected signal intensity will be > 0.028 according to equation (1). By material density reduction (by means of vacuum), this limit may be overcome due to reduction of the electron density and, thus, of the dielectric constant ε. Since $\varepsilon \sim n^2$, then reduction of ε leads to a decrease in the refraction index and, thus, to reflection suppression.

Conclusion

The results of this study show high efficiency of laser treatment of a polymer-based composite material filled with MWCNT for creating anti-reflective surfaces in a wide spectral range ($0.2-25\,\mu$m). This is primarily formation of a particular topology in the near-surface region of specimens

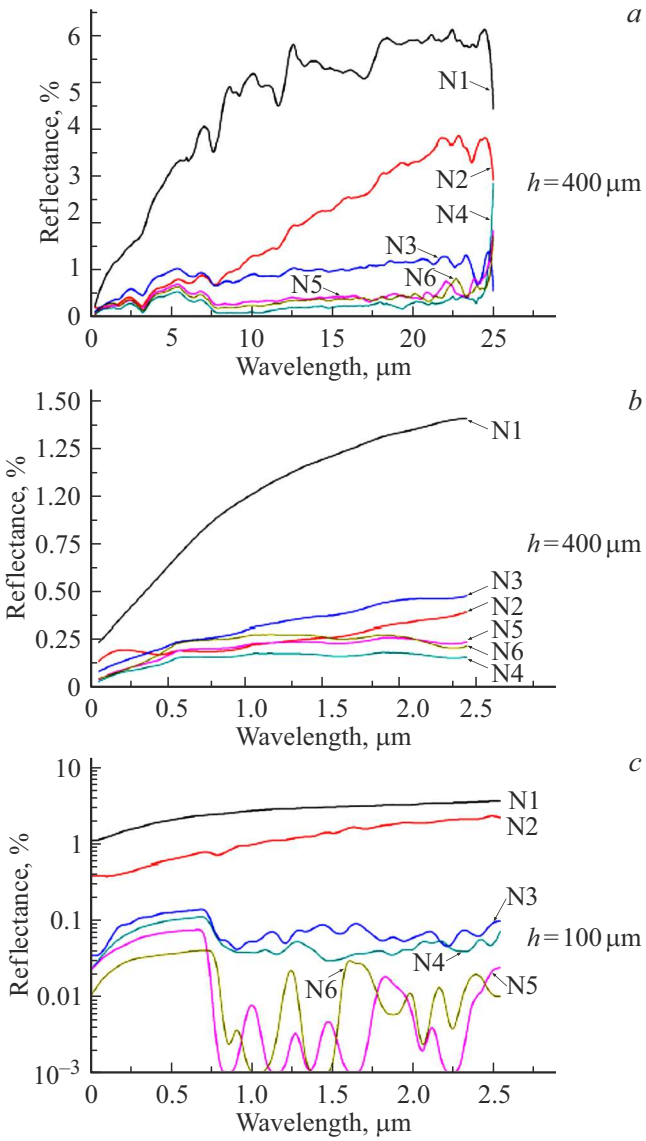

Figure 6. specular reflectance of the initial polymer and composite before and after laser surface treatment in the spectral range of 0.2–25 μm. (*a*) N1 — initial polymer; N2 — composite without structuring; N3 — composite with groove-like surface structuring ($E_p = 12.5$ J, $h = 400\,\mu$m); N4 — composite with pyramid-like surface structuring ($E_p = 12.5$ J, $h = 400\,\mu$m); N5 — composite with groove-like surface structuring ($E_p = 13$ J, $h = 400\,\mu$m); N6 — composite with pyramid-like surface structuring ($E_p = 13$ J, $h = 400\,\mu$m); (*b*) spectra for the same laser exposure parameters in the expanded scale of the spectral range 0.2–2.5 μm; (*c*) spectra for the same laser exposure parameters on the same composite, bur treated with a structuring interval of 100 μm.

that has a refraction index near one and ensures multiple EMR rereflection and absorption. At the same time, formation of microscopic discontinuities and cavities on the groove and pyramid walls, and due to the intrinsic absorbing properties of the Taunite-M MWCNT, performance of such structured materials may be considerable improved. The developed structured composite materials may be used to form anti-reflective coatings for optical and optoelectronic systems on aerospace vehicles as well as for similar ground-based systems.

Acknowledgments

The authors are grateful to I.N. Parkhomenko for discussion of the findings and useful recommendations.

Funding

The study was performed under the National Research Program „Digital and Space Technology, Social and National Security“ (project № 5.1.4.3).

Conflict of interest

The authors declare that they have no conflict of interest.

References

[1] J. Zhu, X. Yang, Z. Fu, C. Wang, W. Wu, L. Zhanbg. J. Porous Mater., **23**(5), 1217 (2016). DOI: 10.1007/s10934-016-0180-5

[2] Y. Lin, J. He. Prog. Mater. Sci., **61**, 94 (2014). DOI: 10.1016/j.pmatsci.2013.12.003

[3] M. Steglich, D. Lehr, S. Ratzsch, T. Kasebier, F. Schrempel, E. Kley, A. Tunnermann. Laser Photonics Rev., **8**(2), L13 (2014). DOI: 10.1002/lpor.201300142

[4] Y. Sun, J. Evans, F. Ding, N. Liu, Y. Zhang, S. He. Opt. Express, **23**(15), 20115 (2015). DOI: 10.1364/OE.23.020115

[5] M. Otto, M. Algasinger, H. Branz, B. Gesemann, T. Gimpel, K. Fuchsel, T. Kasebier, S. Kontermann, S. Koynov, X. Li, V. Naumann, J. Oh, A. Sprafke, J. Ziegler, M. Zik, R. Wehrspohn. Adv. Optical. Mater., **3**(2), 147 (2015). DOI: 10.1002/adom.201400395

[6] F. De Nicola, P. Hines, M. Crescenzi, N. Motta. Phys. Rev. B, **96**, 045409 (2017). DOI: 10.1103/PhysRevB.96.045409

[7] K. Amemiya, D. Fukuda, T. Numata, M. Tanabe, Y. Ichino. Appl. Opt., **51**(29), 6917 (2012). DOI: 10.1364/AO.51.006917

[8] S. Azoubel, R. Cohen, Sh. Mugdassi. Surface and Coatings Technology, **262**, 21 (2015). DOI: 10.1016/j.surfcoat.2014.11.063

[9] D. Das, A. Banerjee. Appl. Surf. Sci., **345**, 204 (2015). DOI: 10.1016/j.apsusc.2015.03.124

[10] C.J. Chunnilall, J.H. Lehman, E. Theocharous, A. Sanders. Carbon, **50**, 5340 (2012). DOI: 10.1016/j.carbon.2012.07.014

[11] J.Y. Liu, M. Soltani, R.K. Dey, B. Cui, R. Lee, H. Podmore. J. Vac. Sci. Technol., **36**(6), 06JG01 (2018). DOI: 10.1116/1.5050986

[12] S. Chuang, H. Chen, J. Shieh, C. Lin, C. Cheng, H. Liu, C. Yu. Nanoscale, **2**, 799 (2010). DOI: 10.1039/C0NR00010H

[13] T. Uchida, M. Moro, S. Hiwasa, J. Taniguchi. In: 2015 *International Conference on Electronics Packaging and iMAPS All Asia Conference (ICEP-IAAC)* (Kyoto, 2015), p. 422. DOI: 10.1109/ICEP-IAAC.2015.7111049

[14] K. Amemiya, H. Koshikawa, T. Yamaki, Y. Maekawa, H. Shitomi, T. Numata, K. Kinoshita, M. Tanabe, D. Fukuda. Nucl. Instr. Meth. Phys. Res. B, **356**, 154 (2015). DOI: 10.1016/j.nimb.2015.05.002

[15] I.N. Parkhomenko, L.A. Vlasukova, I.D. Parfimovich, F.F. Komarov, L.S. Novikov, V.N. Chernik, D.V. Zhigulin. Acta Astronautica, **204**, 124 (2023). DOI: 10.1016/j.actaastro.2022.12.046
[16] W. Sun, A. Du, Y. Feng, J. Shen, S. Huang, J. Tang, B. Zhou. ACS Nano, **10**, 9123 (2016). DOI: 10.1021/acsnano.6b02039
[17] K. Mizuno, J. Ishii, H. Kishida, Y. Hayamizu, S. Yasuda, N. Futaba, M. Yumura, K. Hata. PNAS, **106**(15), 6044 (2009). DOI: 10.1073/pnas.090015510
[18] Z-P. Yang, L. Ci, J.A. Bur, S-Y. Lin, P.M. Ajayan. Nano Lett., **8**(2), 446 (2008). DOI: 10.1021/nl072369t
[19] P.B. Clapham, M.C. Hutrley. Nature, **244**, 281 (1973). DOI: 10.1038/244281a0
[20] A.R. Parker, H.E. Townley. Nat. Nanotechol., **2**, 347 (2007). DOI: 10.1038/nnano.2007.152
[21] O. Zhao, T. Fan, J. Ding, D. Zhang, Q. Guo, M. Kamada. Carbon, **49**, 877 (2011). DOI: 10.1016/j.carbon.2010.10.048
[22] S. J. Wilson, M. C. Hutley. Optica Acta: International J. Optics, **29** (7), 993 (1982). DOI: 10.1080/713820946
[23] S. Ji, J. Park, H. Lim. Nanoscale, **4**, 4603 (2012). DOI: 10.1039/C2NR30787A
[24] J. Lehman, C. Yung, N. Tomlin, D. Conklin, M. Stephens. Appl. Phys. Rev., **5**, 011103 (2018). DOI: 10.1063/1.5009190
[25] Uglerodny nanomaterial „Tunit". [Electronic resource]. URL: http://www.rusnanonet.ru/goods/20235/

Translated by E.Ilinskaya